Quantum transport of Dirac fermions in graphene field effect transistors

V. Hung Nguyen[1,2], A. Bournel[1], C. Chassat[1], and P. Dollfus[1]
[1]Institut d'Electronique Fondamentale, UMR8622, CNRS, Univ. Paris Sud, 91405 Orsay, France
[2]Center for Computational Physics, Institute of Physics, VAST, PO Box 429 Bo Ho, Hanoi 10000, Vietnam
Email: viet-hung.nguyen@u-psud.fr

***Abstract*— We present a quantum transport simulation of graphene field-effect transistors based on the self consistent solution of 2D-Poisson solver and Dirac equation within the non-equilibrium Green's function formalism. The device operation of double gate 2D-graphene field effect transistors is investigated. The study emphasizes the band-to-band and Klein tunneling processes of massless carriers and the resulting features of the electrostatic modulation of I-V characteristics. A transconductance as high as a few hundreds of $\mu S/\mu m$ is observed, despite low on/off current ratios. The model is also extended to massive carriers, which allows us to show the on/off current ratio enhancement due to finite bandgap. The obtained results suggest the feasibility of 2D-graphene devices for analogue applications.**

I. Introduction

Recently, graphene based structures have become the subject of intensive research (see the recent review [1] and references therein) because of their expected potential for applications in nanoelectronics. In comparison with other materials, graphene offers many advantages, such as carrier mobilities of up to 15000 $cm^2\ V^{-1}\ s^{-1}$ at room temperature [2] and large ($\sim 10^8$ A cm^{-2}) critical current densities [3] etc. Differently from conventional semiconductors, graphene is characterized by a zero bandgap and chiral massless carriers. Though it makes difficult the electrostatic control of current, this feature leads to a number of unusual and fascinating transport properties such as finite minimal conductivity, unconventional quantum Hall effect, Klein tunneling [1].

Most recent works on the simulation of electronic transport in graphene transistors are based on either a tight binding or an effective mass description of semiconducting nanoribbons [4, 5]. In ref. [6], we used a non-equilibrium Green's function (NEGF) technique to solve the Dirac equation, which describes the chiral character of massless fermions in 2D-graphene structures. This technique is now self consistently coupled to 2D Poisson's equation to consider double gate graphene FETs. It is also extended to study the transport of massive fermions.

This work was partially supported by the EC through the NoE NANOSIL and by the French ANR through the project NANOSIM-GRAPHENE (ANR-09-NANO-016). V.H.N. acknowledges the MOST of Vietnam for financial support under the project No. 103.02.76.09.

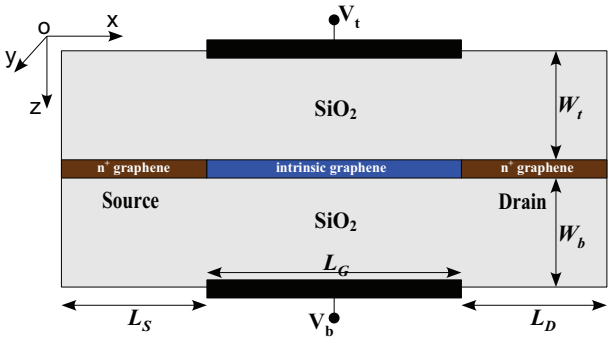

Fig. 1. Schematic cross-section of simulated device. The source and drain extensions are doped to $N_D \approx 10^{13}$ cm^{-2}.

II. Model and Simulation techniques

Close to the zero energy points, massless carriers of 2D graphene are described by the Dirac model [2, 7]

$$H = \mathrm{v}_F \left(p_x\sigma_x + p_y\sigma_y\right) + U_g\left(x\right) \quad (1)$$

where $\mathrm{v}_F \approx 10^6$ m/s is the Fermi velocity, $\vec{p} = (p_x, p_y)$ is the 2D-momentum, $\sigma_{x,y}$ are the Pauli matrices, U_g stands for the potential energy in the graphene channel and is defined by solving the Poisson's equation. We additionally assume that the graphene sheet is large enough for U_g to be just considered as a function of x and the transport along the OY direction to be free. Consistently, it is numerically convenient to represent the Hamiltonian (1) in the basis $\{|x_n\rangle \otimes |k_y\rangle\}$ [6], where k_y denotes the wave vector along the OY direction ($|k_y\rangle = e^{ik_y y}$) and $a = x_{n+1} - x_n$ is the mesh spacing. Hence, the Eq. (1) is rewritten in the matrix form

$$H_{n,l} = \left[U_g\left(x_n\right) + E_y\sigma_y\right]\delta_{l,n} + iE_0\sigma_x\left(\delta_{l,n+1} - \delta_{l,n-1}\right) \quad (2)$$

with $E_0 = \hbar v_F/2a$ and $E_y = \hbar v_F k_y$. Using this tight binding form, it is easy to apply the NEGF to solve the transport equation [6]. In particular, the Green's function is given by

$$G\left(E\right) = \left[\left(E + i0^+\right)I - H - \Sigma_S - \Sigma_D\right]^{-1} \quad (3)$$

where the self energies $\Sigma_{S,D}$ describe the coupling between the graphene channel and the contacts.

The charge density in the channel is then computed by

$$\rho(x) = -2e \int_{-\infty}^{+\infty} dE \int_{-\infty}^{+\infty} dk_y \mathrm{sgn}(E - E_N) \times \{D_S(E,x) f[\mathrm{sgn}(E - E_N)(E - E_{FS})] + D_D(E,x) f[\mathrm{sgn}(E - E_N)(E - E_{FD})]\} \quad (4)$$

where e is the electronic charge, E_N is the charge neutrality level, sgn(E) is the sign function, $E_{FS(FD)}$ is the source (drain) Fermi level, and $D_{S(D)} = G\Gamma_{S(D)}G^\dagger$ with the tunneling rate $\Gamma_{S(D)} = i\left(\Sigma_{S(D)} - \Sigma^\dagger_{S(D)}\right)$ is the local density of states (LDOS) resulting from the source (drain) states. For a self consistent solution, the NEGF transport equation is solved iteratively with the Poisson equation until self consistency is achieved. The current density is then computed by

$$J = \frac{2e}{\pi h} \int_{-\infty}^{+\infty} dE \int_{-\infty}^{+\infty} dk_y \mathcal{T}(E, k_y)[f_S(E) - f_D(E)] \quad (5)$$

where $\mathcal{T}(E) = \mathrm{Trace}\left[\Gamma_S G \Gamma_D G^\dagger\right]$ is the transmission coefficient between the source and the drain.

The simulated device is schematically shown in Fig. 1. The source and drain extensions are doped to $N_D \approx 10^{13} cm^{-2}$ and two gate electrodes are located at distances W_t and W_b, respectively, from the graphene channel. Since the potential U_g is a function of only x, the Poisson equation should be solved in the 2D-space OXZ. Generally, this computation always requires a huge number of grid points because of the open space on the top and bottom of the graphene channel. Therefore, to save the computational cost, the method of moments [8] is used in this work. The advantage of this method is that the grid points are needed only where charge exists. Therefore, the total number of grid points is much smaller than using other methods. The Poisson equation can be written in the integral form as follows

$$\begin{bmatrix} U_g \\ U_c \end{bmatrix} = \begin{bmatrix} K_{gg} & K_{gc} \\ K_{cg} & K_{cc} \end{bmatrix} \begin{bmatrix} \rho_g \\ \rho_c \end{bmatrix} \quad (6)$$

where $[K]$ is the electrostatic kernel, the subscript c (g) denotes the quantities on the contacts (graphene channel). The potential U_g can be obtained directly by solving Eq. (6) when ρ_g (from Eq. (4)) and U_c are known

$$U_g = \left(K_{gg} - K_{gc}K_{cc}^{-1}K_{cg}\right)\rho_g + K_{gc}K_{cc}^{-1}U_c \quad (7)$$

Since the charge density ρ_g depends non-linearly on the potential U_g, it is very efficient to solve this equation by using the Newton-Raphson method [9].

III. Results and Discussion

Using the above formalism, the electrical characteristics of simulated device are investigated. In Fig. 2, we display the self consistent results of (a) the potential profile together with the LDOS ($E_y = 50$ meV), and (b) the electron density. Note that the dispersion relation for Dirac-like carriers defined from the model (1) is $E - U_g = \pm\hbar v_F\sqrt{k_x^2 + k_y^2}$, therefore, for a given

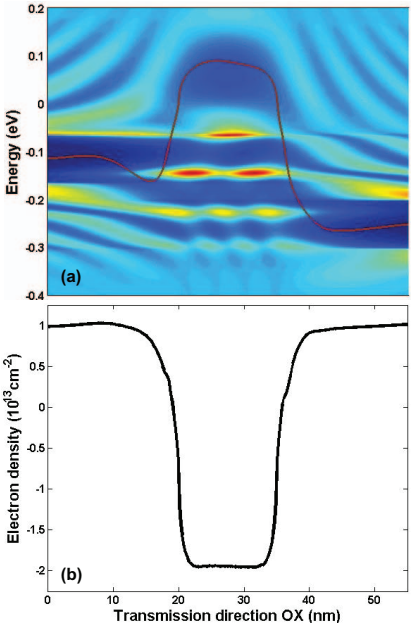

Fig. 2. (a) potential profile (solid line) and corresponding LDOS (for $E_y = 50$ meV), and (b) local electron density (negative values correspond to holes). Everywhere, $L_S = L_D = 20$ nm, $L_G = 15$ nm, $W_t = W_b = 2$ nm, $V_{DS} = 0.2$ V, $V_t = V_b = -1.0$ V, and $T = 77$ K.

energy E_y, the component k_x is imaginary when $|E - U_g| < |E_y|$, i.e., the carrier states are evanescent. Indeed, as shown in Fig. 2(a), an E_y-dependent energy bandgap is formed in the LDOS around the potential energy curve. This bandgap vanishes for normal incident particles ($k_y = 0$). Additionally, in the gated region, the gate voltages induce a potential barrier and generate some hole bound states in the valence band. These hole bound states, as discussed in ref. [6], can give rise to Klein tunneling and resonant features. Actually, due to their chirality, the charge carriers in graphene are both electrons and holes. As a consequence, the electron density presented in Fig. 2(b) exhibits positive (electrons) and negative (holes) values in outside/inside the gated region, respectively. Essentially, this feature concerns with the fact that electrons and holes in graphene are intimately linked and can transform themselves into each other when transmitting through the system [7]. Moreover, because of zero energy bandgap, the band-to-band tunneling, wherein the charge carriers transmit from the valence band (holes, in the left) to the conduction one (electrons, in the right), appears to give a strong contribution to the electrical characteristics of this device [6].

We now explore the I-V characteristics of the device. In Fig. 3, we plot the current density as a function of the bias voltage V_{DS} for different gate voltages. In ref. [10], the authors predicted that the presence of energy gap around the potential barrier U_g can result in a significant negative differential conductance (NDC) in single barrier graphene structures. However, the study in ref. [6] demonstrated that the NDC behavior is not strong because of the contribution of band-to-band tunneling processes. Indeed, our simulation

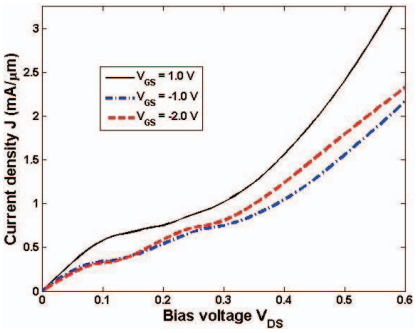

Fig. 3. Current density as a function of bias voltage V_{DS} for different values of V_{GS} ($V_t = V_b \equiv V_{GS}$). Everywhere, $L_S = L_D = 20$ nm, $L_G = 15$ nm, $W_t = W_b = 2$ nm, and $T = 77$ K.

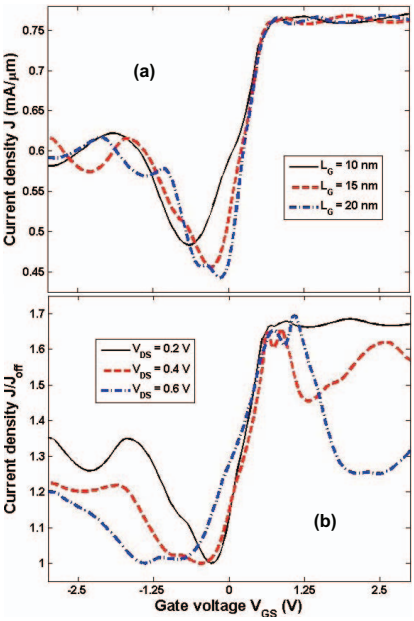

Fig. 4. Current density versus gate voltage for different gate lengths (a) and bias voltages (b). Unless otherwise stated, $L_S = L_D = 20$ nm, $L_G = 15$ nm, $V_{DS} = 0.2$ V, $W_t = W_b = 2$ nm, and $T = 77$ K.

shows that it is difficult to observe the NDC behavior in the simulated device. The existence of the energy gap merely reduces the differential conductance at some bias voltages as seen in Fig. 3. At high bias, the current seems to increase monotonically with the voltage. Additionally, due to confined hole states, some energy gaps between them also appear in the gated region (see in Fig. 2(a)). This leads to the fact that when decreasing the gate voltage (or increasing the height of the potential barrier), some current steps, where the differential conductance is small, can be observed, e.g., as in the I-V curves for $V_{GS} = -1.0$ V and -2.0 V in Fig. 3.

In Fig. 4, we display the current density as a function of the gate voltage. Here, we assume that the same voltage V_{GS} is applied to both two gate electrodes. As seen in the figure, the current density always displays a minimum value at finite negative gate voltage. This minimum point corresponds to the minimum conductance evidenced experimentally [11].

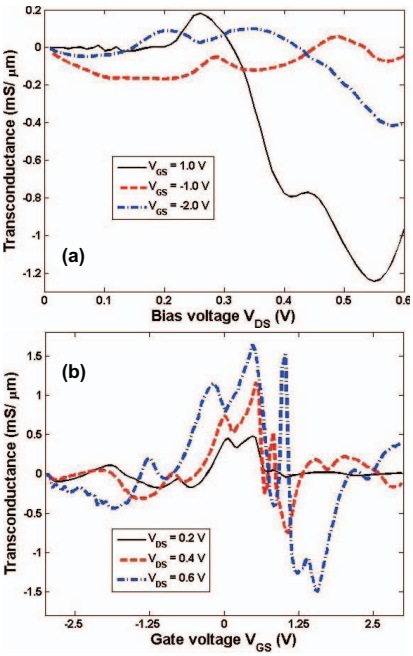

Fig. 5. Transconductance versus bias voltage (a) and gate voltage (b). Everywhere, $L_S = L_D = 20$ nm, $L_G = 15$ nm, $W_t = W_b = 2$ nm, and $T = 77$ K.

Fig. 4(a) shows that while the maximum value of current seems to be unchanged, the minimum current decreases when increasing the gate length. This feature originates from the fact that the minimum current appears when evanescent states around the potential energy U_g in the gated region give important contributions to the current and the transmission via such states decays exponentially as the gate length increases. Therefore, the on/off current ratio, typically $\sim 1.6 \div 2.0$ in Fig. 4, increases with increasing L_G. However, because of zero energy bandgap, this ratio in graphene FETs is very limited, i.e., it is less than 10 [11]. Another important feature observed is the resonant tunneling (Klein tunneling) via hole bound states in the gate-induced barrier region. The tunneling appears when there is a good matching of electron and hole waves outside/inside the barrier, respectively. As a consequence, the current density exhibits a non-trivial structure of resonant peaks when tuning the gate voltage (or potential barrier height), e.g., see the resonant peaks in the negative gate voltage region of Fig. 4(a). In principle, the energy spacing between such resonant peaks reduces when increasing the gate length. Therefore, the effect is smeared and cannot be seen when L_G is large enough [11].

Additionally, the normalized current J/J_{off} as a function of the gate voltage with different bias voltages is plotted in Fig. 4(b). J_{off} is the minimum value of the current in the considered range of the gate voltage. On the one hand, it is shown that the on/off current ratio seems to be unchanged when tuning the bias. On the other hand, the second current valley appears in the positive gate voltage region when the bias increases. The latter feature can be explained as a con-

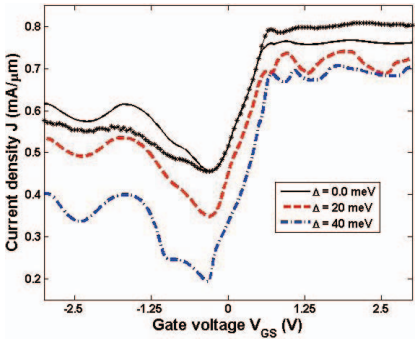

Fig. 6. Current density versus gate voltage for different energy bandgaps Δ. The device parameters are $L_S = L_D = 20$ nm, $L_G = 15$ nm, $V_{DS} = 0.2$ V, $W_t = W_b = 2$ nm, and $T = 77$ K. The star-solid curve corresponds to the results obtained at $T = 300$ K and $\Delta = 0.0$ meV.

sequence of band-to-band tunneling processes in the device. As mentioned above, both Klein tunneling and band-to-band tunneling processes give contributions to the current. However, the latter tunneling processes are important only when the bias is high enough. Essentially, the first (second) current valley originates from the suppression of Klein tunneling (band-to-band tunneling) when the energy gap around the potential barrier U_g moves downward in the energy as schematically illustrated in Fig. 3 of ref. [6]. This also explains the fact that the first and second valleys appear in the negative (potential barrier) and positive (well) gate voltage regions, respectively.

Correspondingly, we display the transconductance as a function of the bias and the gate voltages in Figs. 5(a) and 5(b), respectively. In the case of a gate-induced potential well ($V_{GS} = 1.0$ V), the transconductance is very small at low bias where the band-to-band tunneling is negligible, while it takes high values at high bias where the band-to-band tunneling is important. Fig. 5(a) also shows that the modulation of transconductance by tuning the gate voltage is weak and becomes strong in the low and high bias regions, respectively. Indeed, this point is demonstrated more clearly in Fig. 5(b), where the transconductance versus the gate voltage is plotted for different bias voltages. It is also shown that, on the one hand, the transconductance has both positive and negative values with a high amplitude that can be up to a few hundreds of $\mu S/\mu m$, on the other hand, consistently with the second valley of the current, the transconductance has a deep negative valley at the positive gate voltage region when increasing the bias. Thus, despite the low on/off current ratio, the band-to-band tunneling can result in the high tunability of transconductance by the applied voltages, which is convenient for designing high frequency graphene transistors [11, 12].

Finally, the effects of finite energy bandgap, which can result from the finite width of the graphene sheet [13] and/or from the interaction of the sample with the substrate [14], etc., are displayed in Fig. 6. In this case, the system is no longer described by the massless model but by the massive Dirac model obtaining by adding the mass term $mv_F^2\sigma_z$ into Eq. (1). An important change is that the device is not always transparent for normal incident particles as in the case of massless carriers [7] but the transmission becomes more dependent on the applied voltages. Therefore, when increasing the energy bandgap $\Delta = mv_F^2$, the current density is generally reduced as seen in Fig. 6. Simultaneously, it leads to higher amplitude of transconductance and higher on/off current ratio, e.g., $J_{on}/J_{off} \approx 3.7$ for $L_G = 15$ nm and $\Delta = 40$ meV. The temperature effect is additionally presented in this figure. In principle, increasing the temperature always results in smearing effects, e.g., it blurs the resonant peaks as seen in the case of $T = 300K$. Moreover, consistently with the transport picture described schematically in Fig. 3 of ref. [6], it appears that the current is enhanced/reduced in the cases of a gate-induced potential barrier/well, respectively, when increasing the temperature.

IV. Conclusion

We have developed an efficient self-consistent simulator based on the NEGF method to solve Dirac's equation in 2D graphene devices. The simulator has been then applied to investigate the transport characteristics of a typical double gate graphene FET. It is shown that besides Klein tunneling, the band-to-band tunneling is very important in this device. As a consequence, the on/off current ratio is very limited, i.e., it is less than 10. However, the electrostatic modulation of the channel can yield transconductance values as high as a few hundreds of $\mu S/\mu m$. An additional energy bandgap can reduce the current and simultaneously make the on/off current ratio as well as the amplitude of transconductance higher. Therefore, though not suitable for digital applications, these device characteristics may be convenient for analogue circuit applications [11, 12].

Acknowledgment

The authors would like to thank H. Nha Nguyen, V. Nam Do and V. Lien Nguyen for very useful discussions.

References

[1] A. H. Castro Neto, F. Guinea, N. M. R. Peres, K. S. Novoselov, and A. K. Geim, Rev. Mod. Phys. **81**, 109 (2009).
[2] A. K. Geim and K. S. Novoselov, Nat. Mater. **6**, 183 (2007).
[3] K. S. Novoselov, A. K. Geim, S. V. Morozov, D. Jiang, Y. Zhang, S. V. Dubonos, I. V. Grigorieva, A. A. Firsov, Science **306**, 666 (2004).
[4] G. Fiori and G. Iannaccone, IEEE Electron Device Lett. **28**, 760 (2007).
[5] R. Grassi, S. Poli, E. Gnani, A. Gnudi, S. Reggiani, and G. Baccarani, Solid State Electron. **53**, 462 (2009).
[6] V. Nam Do, V. Hung Nguyen, P. Dollfus, and A. Bournel, J. Appl. Phys. **104**, 063708 (2008).
[7] M. I. Katsnelson, K. S. Novoselov, and A. K. Geim, Nat. Phys. **2**, 620 (2006).
[8] J. Guo, S. Datta, M. P. Anantram, and M. Lundstrom, J. Comput. Electron. **3**, 373 (2004).
[9] Z. Ren, Ph.D Thesis, Purdue University, West Lafayette, 2001.
[10] D. Dragoman and M. Dragoman, Appl. Phys. Lett. **90**, 143111 (2007).
[11] I. Meric, M. Y. Han, A. F. Young, B. Ozyilmaz, P. Kim, and K. L. Shepard, Nat. Nanotechnol. **3**, 654 (2008).
[12] Y.-M. Lin, K. A. Jenkins, A. Valdes-Garcia, J. P. Small, D. B. Farmer and P. Avouris, Nano Lett. **9**, 422 (2009).
[13] M. Y. Han, B. Ozyilmaz, Y. Zhang, and P. Kim, Phys. Rev. Lett. **98**, 206805 (2007).
[14] S. Y. Zhou, G.-H. Gweon, A. V. Fedorov, P. N. First, W. A. de Heer, D.-H. Lee, F. Guinea, A. H. Castro Neto, and A. Lanzara, Nat. Mater. **6**, 770 (2007).